Coupled Fluid-Structure Interaction Analysis of Solid Rocket Motor with Flexible Inhibitors

H. Q. Yang[1]
CFD Research Corp./Jacobs ESSSA Group

Jeff West[2]
Fluid Dynamics Branch-ER42
George C. Marshall Space Flight Center
and

Robert E. Harris[3]
CFD Research Corporation

Flexible inhibitors are generally used in solid rocket motors (SRMs) as a means to control the burning of propellant. Vortices generated by the flow of propellant around the flexible inhibitors have been identified as a driving source of instabilities that can lead to thrust oscillations in launch vehicles. Potential coupling between the SRM thrust oscillations and structural vibration modes is an important risk factor in launch vehicle design. As a means to predict and better understand these phenomena, a multidisciplinary simulation capability that couples the NASA production CFD code, Loci/CHEM, with CFDRC's structural finite element code, CoBi, has been developed. This capability is crucial to the development of NASA's new space launch system (SLS). This paper summarizes the efforts in applying the coupled software to demonstrate and investigate fluid-structure interaction (FSI) phenomena between pressure waves and flexible inhibitors inside reusable solid rocket motors (RSRMs). The features of the fluid and structural solvers are described in detail, and the coupling methodology and interfacial continuity requirements are then presented in a general Eulerian-Lagrangian framework. The simulations presented herein utilize production level CFD with hybrid RANS/LES turbulence modeling and grid resolution in excess of 80 million cells. The fluid domain in the SRM is discretized using a general mixed polyhedral unstructured mesh, while full 3D shell elements are utilized in the structural domain for the flexible inhibitors. Verifications against analytical solutions for a structural model under a steady uniform pressure condition and under dynamic modal analysis show excellent agreement in terms of displacement distribution and eigenmode frequencies. The preliminary coupled results indicate that due to acoustic coupling, the dynamics of one of the more flexible inhibitors shift from its first modal frequency to the first acoustic frequency of the solid rocket motor. This insight could have profound implications for SRM and flexible inhibitor designs for current and future launch vehicles including SLS.

Nomenclature

a	=	burning rate constant
D	=	bending rigidity of a plate
[D]	=	damping matrix
f	=	internal body force
[G]	=	transformation matrix
k	=	thermal conductivity
[K]	=	stiffness matrix

[1] Chief Scientist, CFD Research Crop., 701 McMillian Way, Huntsville, AL 35806, AIAA Senior Member
[2] Team Lead, Fluid Dynamics Branch-ER42, George C. Marshall Space Flight Center, AL 35812, AIAA Member
[3] Principal Engineer, CFD Research Corp., 701 McMillian Way, Huntsville, AL 35806, AIAA Senior Member

M	=	plate mass per unit area
[M]	=	mass matrix
p	=	pressure
r	=	radial coordinate
R	=	radius of a plate
R	=	universal gas constant
t	=	time
u	=	velocity component
w	=	deflection of a plate
v	=	velocity vector
T	=	temperature
Vol	=	control volume
x	=	Eulerian coordinate
X	=	Lagrangian coordinate

subscripts

s	=	in the solid phase
f	=	in the fluid phase
fs	=	on fluid-solid interface
G	=	moving grid part
i	=	direction in x, y, or z
n	=	normal direction
τ	=	tangential direction

symbols

ρ	=	density
σ	=	stress tensor
λ,η	=	Lamé constant
τ	=	shear stress
μ	=	dynamic viscosity of fluid
χ	=	mesh coordinate

1. Introduction

During the development of Ares I and Ares V launch vehicles, potential coupling between thrust oscillations in the solid rocket motor (SRM) first stage and vibration modes in the launch vehicle was identified as the top risk in the Ares I program. The frequency of pressure pulses in the five-segment SRM is close to the natural frequency of the second longitudinal vibration mode of the complete launch vehicle. This creates the risk of a "pogo stick" resonant vibration, which leads to concerns that the vibration could make it difficult for the astronaut to perform their tasks, including reading their flight displays. As the thrust oscillations come mainly from solid rocket motor pressure oscillations, an accurate predictive capability of pressure oscillation features considering all the important driving physics is crucial in the development of NASA's new space launch system (SLS).

Vortices emitted by an obstacle such as an inhibitor have been identified as the driving acoustic and combustion instability sources that can lead to thrust oscillations from the SRM. Flexible inhibitors have been used in the space shuttle reusable solid rocket motor (RSRM) to control the burning of propellant as illustrated in Figure 1.[1] The inhibitor is an insulating material bonded to part of the propellant that prevents the underlying surface from becoming hot enough to ignite. The RSRM has inhibitors on the flat, forward-facing ends of the propellant in each of the 3 joint slots, which are annular rings made of asbestos-silica-filled nitrile butadiene rubber (NBR). The inhibitors help fine-tune the burning surface area, and therefore the thrust performance, to satisfy Shuttle requirements.[1]

American Institute of Aeronautics and Astronautics
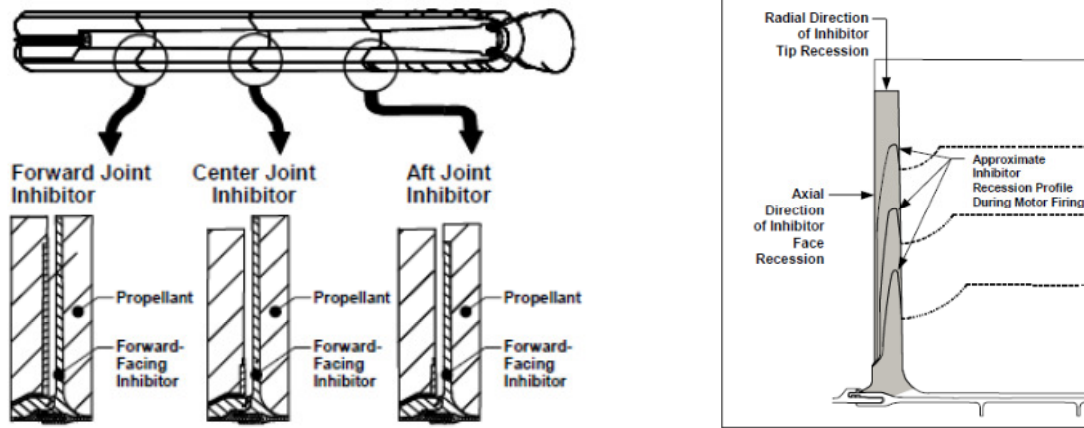
(a) RSRM propellant and inhibitor configuration for each field joint.

(b) General direction of RSRM inhibitor material recessions.

Figure 1. Flexible Inhibitors inside NASA's Space Shuttle Reusable Solid Rocket Motor.[1]

The presence of an inhibitor can significantly affect the flow field in its immediate vicinity and some distance downstream, primarily through vortex shedding from the inhibitor tip. A number of cold-flow experiments and high fidelity numerical simulations have been performed to study the influence of inhibitors on pressure oscillations in rockets.[2,3,4] A recent study by Mastrangelo *et al.*,[5] has identified the inhibitor as the main source of amplification of the pressure oscillation.

Since inhibitors often consist of relatively thin sheets of flexible materials, the difference in gas pressure on the forward- and aft-facing sides of the protruding portion of an inhibitor can cause it to bend in the direction of the flow. If the inhibitor is long and compliant enough, it can come into contact with the burning propellant surface downstream. Even if the inhibitor does not contact the propellant surface, it can be expected to oscillate about some equilibrium angle of deflection if viscoelastic damping in the solid and viscous damping from the fluid are small enough. It is very important to understand the role of the flexible inhibitors in the coupling physics. For instance, does the inhibitor flexibility lead to the instability or does the flexibility of the inhibitor act as a means of controlling and reducing unstable modes in the SRM? For turbulent flow inside the SRM, the load on the inhibitor is generally highly 3D and chaotic and therefore very complex inhibitor motions are possible even if the material is isotropic and undamaged. It is important to understand not only the effect of inhibitor shape on the vortex shedding but also how the dynamically changing inhibitor geometry affects the flow.

Roach *et al.*[6,7] made attempts to study the flexible inhibitor interacting with a firing rocket motor using a quasi-static coupling approach. First, a static or time-dependent fluid-only computation was performed on the initial inhibitor geometry. The resulting pressure load was passed (through files) to a commercial finite element method (FEM) solver, which determined the deformation under that prescribed load. The new geometry was passed (through files) back to the fluid solver, and the steady or unsteady flow was determined from the new geometry. Fiedler *et al.*[8] successfully computed the motion of a flexible inhibitor located in the core flow region aft of a joint slot in a fully coupled 3D simulation. They demonstrated that an inhibitor flapped periodically with an angle of deflection ranging from 30 to 40 degrees. Unfortunately, no information regarding such a flapping effect on the instability mechanism is available. Wasistho *et al.*[9] conducted a numerical study of 3D flows past rigid and flexible inhibitors in the space shuttle redesigned solid rocket motor (RSRM). Only a section of the rocket near the center joint slot at 100 seconds after ignition was modeled using compressible dynamic large eddy simulation (LES) for the fluid domain and an implicit finite element solver for the solid domain. Differences in the instantaneous and mean flow response to rigid and flexible inhibitors led to some useful insights regarding the design of inhibitor geometry and material.

As of this writing, no fully-coupled fluid-structure interaction simulation has been reported for a production-level (50 – 500 million cells) SRM study, and no mature tool to analyze and study the fluid-structure interaction in a solid rocket motor exists on a production level. In a recent study, a comprehensive, fully-coupled, high fidelity, user-friendly multi-disciplinary simulation tool was developed by CFD Research Corp. (CFDRC) and Mississippi State University[10] to enable the investigation of the nonlinear interaction of flexible inhibitors with the vortical flow inside the SRM. The approach was to couple a NASA production CFD code, Loci/CHEM, for solid rocket motor ignition

analysis (see the sample result in Figure 2a) with a DoD Open Source Finite Element Analysis code, CoBi, developed at CFDRC for nonlinear large structural deformation (see example in Figure 2b).
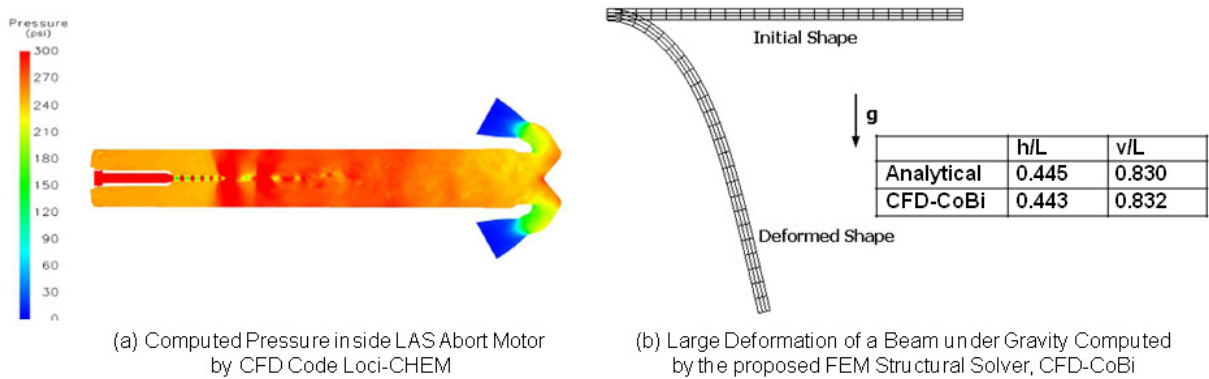

(a) Computed Pressure inside LAS Abort Motor
by CFD Code Loci-CHEM

(b) Large Deformation of a Beam under Gravity Computed
by the proposed FEM Structural Solver, CFD-CoBi

Figure 2. Capability demonstration for CFD: Loci/CHEM and for Computational Structural Dynamics (CSD): CoBi.

The simulation tool with the above features is a highly valuable asset when the time comes to design a new motor or even when a modification is planned on existing geometries. The multi-disciplinary tool can improve pressure oscillation modeling fidelity and provide insight into nonlinear fluid-structure interaction leading to thrust oscillations in the preliminary design phase for future SRM for SLS. The present tool is also useful in identifying and predicting, as a first approximation and at a very early stage, the critical geometries and the time during firing at which thrust oscillations could occur.

II. Mathematical Formulation

Continuum mechanics has been conventionally subdivided into the distinct fields of solid mechanics and fluid mechanics. Even though both disciplines solve Newton's second law of motion, they use different reference frames, as well as different solution variables and solution methods. For example, in structural dynamics, the dependent variables are displacements, and are typically formulated in a Lagrangian reference frame. These displacements are solved by finite element method (FEM). In fluid dynamics, the dependent variables are velocities, pressure, density, etc., and are typically formulated in an Eulerian reference frame and solved using the finite volume method (FVM) or finite difference method (FDM). Some of the characteristics of fluid dynamics and structural dynamics solvers are listed in Table 1.

As a result, problems involving interaction between fluid flow and solid deformation, with the examples of an aircraft body and wing, wind loaded structure and heat transfer, are generally treated separately and in a decoupled manner. There is, however, a wide range of problems that require simultaneous solution of fluid flow and solid body deformation, and thus require a unified multidisciplinary approach. This section will first present a unified formulation for both fluid and structure, and then describe the fluid and structural solvers used in this study. Finally the coupling methodology of the solvers will be discussed.

A.   Unified Governing Equation

Regardless of the solution method (FEM, FVM, or FDM), the solid and fluid mechanics actually share the same governing equations, and differ only in constitutive relations. The governing equations for both a fluid and a solid are the momentum equations of Newton's law:

$$\rho \dot{v}_i = \sigma_{ij,j} + f_i \tag{1}$$

where ρ is the density, v_i is the velocity, σ_{ij} is the stress tensor, f_i is the internal body force, a superscript dot designates a total derivative, a comma denotes a partial derivative with respect to the following variable, and

repeated indices denote summation over the appropriate range. To close the system in Eq. (1), information about the response of a particular material to an applied force is necessary. Here we will take a compressible gas and elastic solid as example of fluid and solid materials, respectively.

Table 1. Comparison of fluid dynamics and structural dynamics solutions.

	Fluid Dynamics	Structural Dynamics
Reference Frame	Eulerian	Lagrangian
Discretization	Finite Volume Method	Finite Element Method
Solution Variables	Velocity v_x, v_y, v_z	Displacement u_x, u_y, u_z
Equation Type	Parabolic or Elliptic	Hyperbolic
Unknown Location	Cell Center	Cell Node
Expression for Acceleration, a	$\dfrac{d\vec{V}}{dt} = \dfrac{\partial \vec{V}}{\partial t} + \dfrac{\partial \vec{V}}{\partial x}\dfrac{\partial x}{\partial t} = \dfrac{\partial \vec{V}}{\partial t} + (\vec{V}\cdot\nabla)\vec{V}$	$\dfrac{d\vec{V}}{dt} = \dfrac{\partial \vec{V}}{\partial t}$
Solvers	Loci/CHEM, Loci/STREAM	Nastran
Constitutive Relation	Proportional to Velocity Gradient	Proportional to Displacement Gradient

For fluid dynamics:

The equation of state is:

$$\rho = \rho(p, T) \tag{2}$$

where p is pressure and T is temperature. For an incompressible fluid :

$$\rho = \text{constant} \tag{3}$$

and for an ideal gas:

$$\rho = \frac{p}{RT} \tag{4}$$

The constitutive relation between stress and rate of deformation for fluids is given by Stokes' law:

$$\sigma_{ij} = \mu\left(v_{i,j} + v_{j,i}\right) - \frac{2}{3}\mu\,\delta_{ij}v_{k,k} - p\delta_{ij} \tag{5}$$

where μ is the dynamic viscosity.

For an elastic solid:

The constitutive relationship is given by Hooke's law:

$$\sigma_{ij} = \eta\left(u_{i,j} + u_{j,i}\right) + \lambda\delta_{ij}u_{k,k} \tag{6}$$

where η and λ are the Lamé constants, u_i is the displacement vector and

$$v_i = \dot{u}_i \tag{7}$$

Note that in the fluid the stress is expressed in terms of velocity, whereas in the solid the stress is expressed in terms of displacement.

B. Consistent Interface Boundary Conditions

As for boundary conditions at the fluid-solid interface, it is required that displacement, velocity and stresses are continuous, i.e.

$$\left(u_i\right)_s = \left(u_i\right)_f \tag{8}$$

$$\left(v_i\right)_s = \left(v_i\right)_s \tag{9}$$

$$\left(\left(\sigma_{ij}\right)_n\right)_s = \left(\left(\sigma_{ij}\right)_n\right)_f \tag{10}$$

$$\left(\left(\sigma_{ij}\right)_\tau\right)_s = \left(\left(\sigma_{ij}\right)_\tau\right)_f \tag{11}$$

with subscript s and f representing solid and fluid domains, and n and τ are the normal and tangential directions with respect to the interface.

C. Reference Frame and Mesh Systems

Before an equation is discretized, it is important to select an appropriate reference frame. In classical solid mechanics, the dynamics equation is formulated in a Lagrangian reference frame, where:

$$\rho\dot{v}_i = \rho\frac{dv_i}{dt} \tag{12}$$

Here one moves with or follows the structure. In classical fluid dynamics, the conservation equation is formulated in an Eulerian frame, where:

$$\rho\dot{v}_i = \rho\frac{\partial v_i}{\partial t} + v_{i,j}v_j \tag{13}$$

It is the second nonlinear term that has given rise to many difficulties in fluid dynamics. However, in the fluid dynamics approach, the Eulerian frame is necessary. To distinguish the difference between the two reference frames, we denote the space (Eulerian) coordinate by x_i, the material (Lagrangian) coordinate by X_i, and mesh coordinate by χ_i. Then if our mesh is given by

$$\chi_i = x_i \tag{14}$$

we have identified an Eulerian mesh and when

$$\chi_i = X_i \tag{15}$$

is used, we are identifying a Lagrangian mesh.

D. Eulerian-Lagrangian (Fluid) - Lagrangian (Solid) Approach

Since the structural dynamics equations are formulated in a Lagrangian reference frame whereas the fluid dynamics equations are formulated in an Eulerian reference frame, direct coupling of two solvers could lead to overlapped meshes or holes in the solution domain. This is illustrated in Figure 3.

Original fluid and solid meshes | Meshes after structure deformation | Meshes using Eulerian-Lagrangian
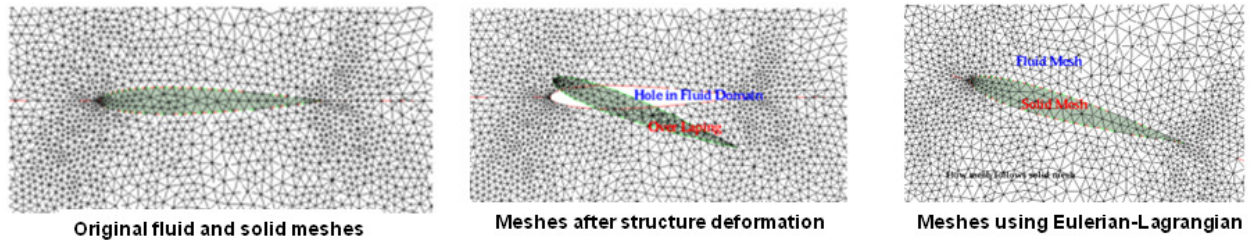
Figure 3. Mesh deformation for Eulerian and Eulerian-Lagrangian approach.

The critical requirement for reference frames is to preserve fluid-structure interface and prevent cutting and crossing. This ensures that consistent interface conditions are applied. The Eulerian-Lagrangian (fluid) - Lagrangian (solid) approach has the above properties as seen from Figure 3. Within this formulation, a mesh velocity is introduced and the momentum equation becomes:

$$\rho \frac{\partial v_i}{\partial t} + \left(v_j - v_{Gj}\right)v_{i,j} = \sigma_{ij,j} + f_i \tag{16}$$

Here we set the mesh velocity as:

$$v_{Gj} = v_j \text{ in the solid} \tag{17}$$

$$\left(v_{Gj}\right)_{fs} = \left(v_j\right)_{fs} \text{ at the solid-fluid interface} \tag{18}$$

To facilitate the Eulerian-Lagrangian framework for the fluid, a volumetric mesh deformation in the fluid domain is required.

III. Solution Procedure

A. Fluid Dynamics Solver

A fully-coupled fluid-structure interaction approach requires solvers for both fluid and structural phases. A NASA production CFD code, Loci/CHEM, is used to solve the compressible fluid dynamics inside the solid rocket motor. The Loci/CHEM code is a modern multiphysics simulation code that is capable of modeling chemically reacting multiphase high- and low-speed flows. CHEM, which was developed at Mississippi State University, is written in the Loci framework[11] and is a Reynolds-averaged Navier-Stokes, finite-volume flow solver for generalized arbitrary polyhedral grids. The Loci system uses a rule-based approach to automatically assemble the

numerical simulation components into a working solver. This technique enhances the flexibility of simulation tools, reducing the complexity of CFD software introduced by various boundary conditions, complex geometries, and varied physical models. Loci plays a central role in building flexible goal-adaptive algorithms that can quickly match numerical techniques with various physical modeling requirements. Loci/CHEM is also equipped with a robust volume mesh deformation module that is capable of efficiently resolving large-scale deformations in the fluid mesh as a result of boundary motion or deformation.

Loci/CHEM[12] uses density-based algorithms and employs high-resolution approximate Riemann solvers to solve finite-rate chemically reacting viscous turbulent flows. It supports adaptive mesh refinement, simulations of complex equations of state including cryogenic fluids, multiphase simulations of dispersed particulates using both Lagrangian and Eulerian approaches, conjugate heat transfer through solids,[13] and non-gray radiative transfer associated with gas and particulate phases. It supports multiple two-equation RANS turbulence models including Wilcox's k-ω model, Menter's baseline model, and Menter's shear stress transport model (SST).[14] For unsteady flow problems such as the present rocket motor acoustic waves, Loci/CHEM has hybrid RANS/LES turbulence model treatments that include high speed compressibility corrections. The Loci/CHEM CFD code is a library of Loci rules (fine-grained components), and provides primitives for generalized meshes, including metrics; operators, such as gradient; chemically reacting physics models, such as equations of state, inviscid flux functions, and transport functions (viscosity, conduction, and diffusion); a variety of time and space integration methods; linear system solvers; and more. Moreover, it is a library of reusable components that can be dynamically reconfigured to solve a variety of problems involving generalized meshes by changing the given fact database, adding rules, or changing the query. Using the sophisticated automatic parallelization framework of Loci, Loci/CHEM has demonstrated scalability to problems in size exceeding five hundred million cells and production scalability to four thousand processors.

B. Nonlinear Structure Dynamics Solver

The structural dynamics solver used in this study, CoBi, is a DoD Open Source code developed at CFDRC. CoBi discretizes the Eq. (1) using the finite element method as:

$$[M]\frac{\partial^2 \{u_s\}}{\partial t^2} + [D]\frac{\partial \{u_s\}}{\partial t} + [K]\{u_s\} = \{f_s\} \tag{19}$$

where M, v_s, D, K, u_s, f_s denote the mass matrix, the velocity, the damping matrix, the stiffness matrix, the displacements, and the loads, respectively. The main capabilities of the solver include:
- triangular, quadrilateral, tetrahedral, prismatic, or brick elements
- linear or high-order isoparametric elements;
- small or large deformations;
- elastic or plastic stresses;
- isotropic or anisotropic materials;
- thin to thick shell/plate elements;
- modal analysis and eigenvalue solutions; and
- steady and dynamic analysis.

To consider the large deformation of the inhibitor, the nonlinear strain due to large deformations must be taken into account. The nonlinear structural effect can shed light on the complex coupling of acoustics with structural vibrations, which is not available in classical linear analysis. Typically, for the elastic solid, the linear constitutive relationship is given by Hooke's law (Eq. (6)):

$$\sigma_{ij} = \eta(u_{i,j} + u_{j,i}) + \lambda\delta_{ij}u_{k,k} \tag{20}$$

where η and λ are the Lamé constants and u_i is the displacement vector. A comma denotes a partial derivative with respect to the following variable. To include the nonlinear geometrical contribution, additional terms have to be added such that:

$$\sigma_{ij} = \eta\big[[(u_{i,j} + u_{j,i} + u_{k,j}u_{j,k}) + \lambda\delta_{ij}(u_{k,k} + u_{m,k}u_{m,k})]\big] \tag{21}$$

To expand the above expression, for example, the strain-displacement for ε_x and ε_{xy} can be written as:

$$\varepsilon_x = \frac{\partial u}{\partial x} + \frac{1}{2}\left[\left(\frac{\partial u}{\partial x}\right)^2 + \left(\frac{\partial v}{\partial x}\right)^2 + \left(\frac{\partial w}{\partial x}\right)^2\right] \tag{22}$$

$$\varepsilon_{xy} = \frac{\partial u}{\partial x} + \frac{\partial v}{\partial y} + \left[\frac{\partial u}{\partial x}\cdot\frac{\partial u}{\partial y} + \frac{\partial v}{\partial x}\cdot\frac{\partial v}{\partial y} + \frac{\partial w}{\partial x}\cdot\frac{\partial w}{\partial y}\right] \tag{23}$$

Similar expressions can be written for the other strain components. The nonlinear terms in the above expression are due to geometrically large deformations. As such, the structural dynamics equation is no longer linear. In this study, the final nonlinear equation is solved by Newton's method in the FEM module, where the stiffness matrix is represented as:

$$[k] = [k_o] + [k_\sigma] + [k_L] \tag{24}$$

in which: $[k_o]$ is the linear small displacement stiffness matrix;
$[k_\sigma]$ is a symmetric matrix dependent on the stress level; and
$[k_L]$ is known as the initial displacement matrix.

C. Fluid-Structure Coupling and Data Exchange

The coupling of the structural dynamics solver, CoBi, with the fluid dynamics solver, Loci/CHEM, is accomplished through the boundary conditions across the solid-fluid interface. The boundary conditions require the continuity of interface displacement and velocity, and the continuity of normal and tangential forces, as stated in Eqs. (8)-(10). Since each solver (structural and fluid) employs an iterative method within each time step, coupling across the interface is carried out at the inner iteration level ensure strong coupling. Within each physical time step, the flow solution and the structural solution are repeatedly advanced by several iterations followed by an update of the aerodynamic forces and mesh deformations. This procedure is repeated until the flow and displacements are converged before proceeding to the next physical time step. This modular treatment allows one to apply well-established and optimized methods for the both flow and the structure solution, respectively.

In practical applications, the CFD model may use a much finer discretization than does the CSD model. As a result, the mesh used for discretization of the structural mode shapes does not coincide with the flow mesh as shown in Figure 4. In our current study, aerodynamic loads are obtained on the body-matched flow mesh and are projected onto the structural mesh. Deformations obtained on the structural mesh must then be transferred to the flow mesh. Both transformations have to satisfy the requirements of conservation of work and energy.
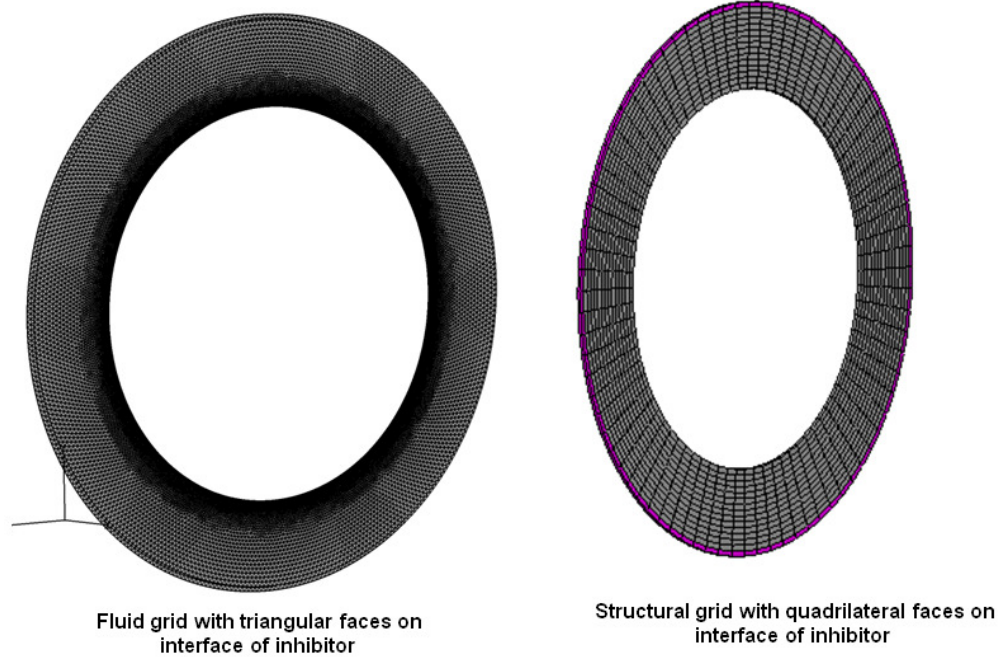
Fluid grid with triangular faces on
interface of inhibitor

Structural grid with quadrilateral faces on
interface of inhibitor

Figure 4. Illustration of non-matching interface between fluid mesh (left) and structure mesh (right).

The principle of virtual work is employed to ensure conservation. For a linear transformation, let the displacements $\{x_a\}$ of the fluid mesh to be expressed in terms of the structural mesh displacements $\{x_s\}$ using a transformation matrix $[G]$:

$$\{x_a\} = [G]\{x_s\} \tag{25}$$

then the requirement for conservation leads to a corresponding matrix for the transformation of forces:

$$\{f_s\}^T\{\Delta x_s\} = \{f_a\}^T\{\Delta x_a\} = \{f_a\}^T[G]\{\Delta x_s\} \tag{26}$$

which leads to:
$$\{\Delta f_s\}^T = [G]^T\{\Delta f_a\} \tag{27}$$

In this way, the global conservation of work can be satisfied regardless of the method that is used to obtain the transformation matrix. In the current coupling procedure, Loci/CHEM provides traction vectors at face centers which are then interpolated to nodal forces on an interface mesh in the CoBi model through the above transformation.

IV. Model Description

We now apply the tightly-coupled fluid-structure interaction capabilities to simulate the flow and structural response inside the RSRM with flexible inhibitors separating the propellant sections. The computational model is a RSRM at 80 seconds after ignition as shown in Figure 5. The model is comprised of a propellant grain surface, solid walls, and exit boundaries. All geometrical models, boundary conditions, and initial conditions are based on the work by Phil Davis of NASA MSFC at ER42.[15]

A. Fluid Dynamics Mesh

An initial unstructured hybrid prism/pyramid/tet/hex computational mesh comprised of 62.5M cells was generated for this application. The solid rocket motor was meshed using 1 inch surface spacing for the grain and

American Institute of Aeronautics and Astronautics

walls. Finer spacing was used at the inhibitors and coarse spacing was used downstream of the throat. An illustration of a cross-sectional cut through the computational mesh is given in Figure 5.
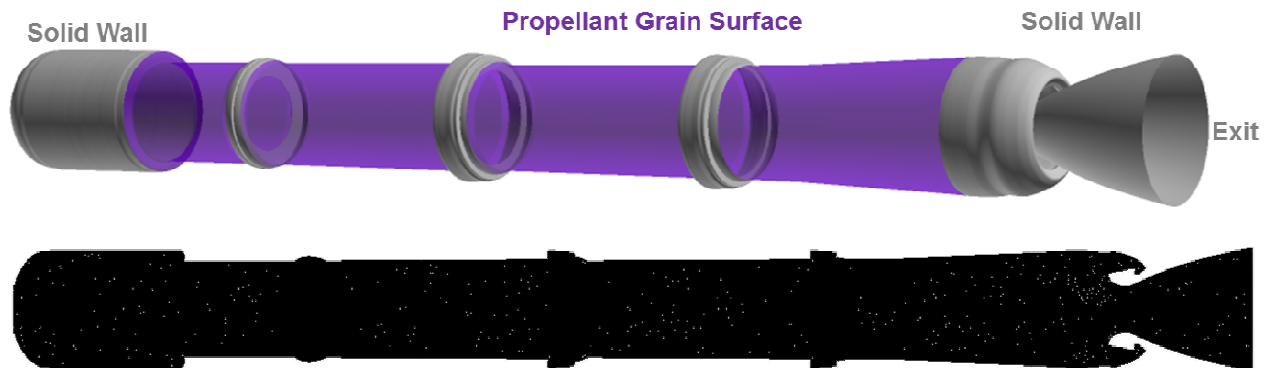

Figure 5. Geometry for reusable solid rocket motor (RSRM) problem: (Top) Illustration of propellant grain surface, solid wall, and exit boundaries; (Bottom) Cross-sectional cut of 3D mesh.

To better capture and preserve vortices shed from the inhibitors, a finer mesh was also generated where cells were packed near the path of the vortex street from the inhibitors as shown in Figure 6. The new mesh keeps the same spacing on the grain and solid wall surfaces with a total cell count of 80 Million.
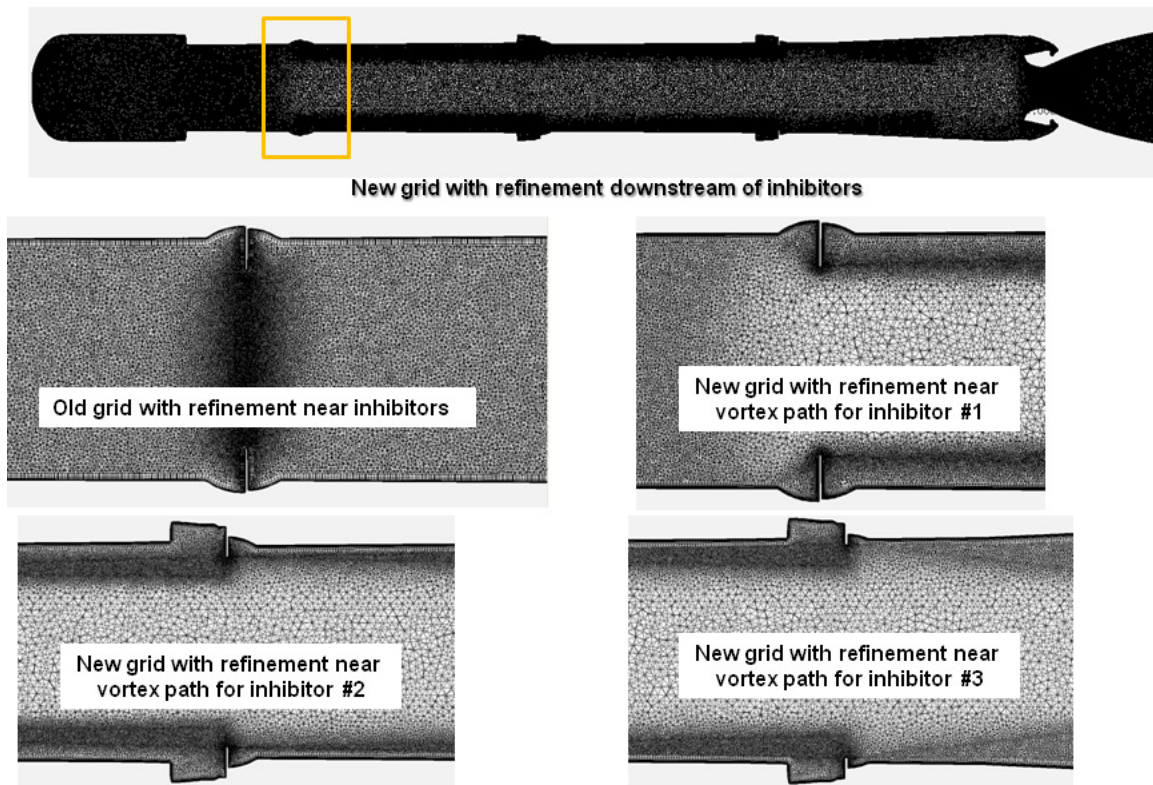
Figure 6. The refined mesh with packed cells near the vortex path for three inhibitors.

B. Fluid Dynamics Solver Settings

For the Loci/CHEM flow solution, 2nd order spatial and temporal accuracy is employed, with the 2nd order upwind inviscid flux and Venkatakrishnan limiter. A time step of 0.0001s is used with 8 Newton iterations per time step, and urelax=0.4. Sutherland's law is applied as the laminar transport model, and Mentor shear stress transport (SST) turbulence model with multi-scale LES is employed. Since direct numerical simulation (DNS) calculations are impractical for complex flows and RANS calculations are not strictly applicable to unsteady flows, the technique of combining traditional RANS with large eddy simulation (LES) (hybrid RANS/LES) offers an affordable alternative. With hybrid RAN/LES, only the largest turbulent eddy structures that can be adequately resolved on a given mesh are simulated. The smallest remaining structures and the turbulence energy contained within them are then modeled using a sub-grid-scale model. This technique allows a more appropriate representation of the unsteady turbulent fluctuations than RANS alone, and it is computationally feasible for the present unsteady flow with vortex shedding and breakdown.

A single phase equivalent gas model is used as the chemistry model for the RSRM gas.[15] An adiabatic, no-slip boundary condition is employed on all solid walls and a supersonic outflow condition is employed at the exit. On the propellant grain surfaces, gas at 3,996K is injected in the normal direction into the fluid domain with a mass flux determined from the steady burn-rate formula of:

$$\dot{m} = \rho_s a P^n \tag{28}$$

Here, ρ_s is propellant density; a is the burning rate constant, and n is constant.

C. Structural Dynamics Mesh

The computational meshes for the finite element solution on the three flexible inhibitors are shown in Figure 7. All three inhibitor meshes are comprised of 80 cells in the circumferential direction, and 1 cell in the axial direction, with 14, 10, and 7 cells in the axial direction for the 1st, 2nd, and 3rd inhibitor, respectively. As the inhibitor is very thin, the problem is solved using the shell element formulation. The above discretization yields 1120, 800 and 560 shell elements for the 1st, 2nd, and 3rd inhibitor, respectively. Unlike the fluid mesh, where the smallest vortex could dominate the fluid physics such as in turbulent flow, in structural dynamics the first few modal deformations dominate the structural response. Due to this property, it is possible to use a much coarser mesh for the structural solution. The results for the modal analysis are presented in Section 5.
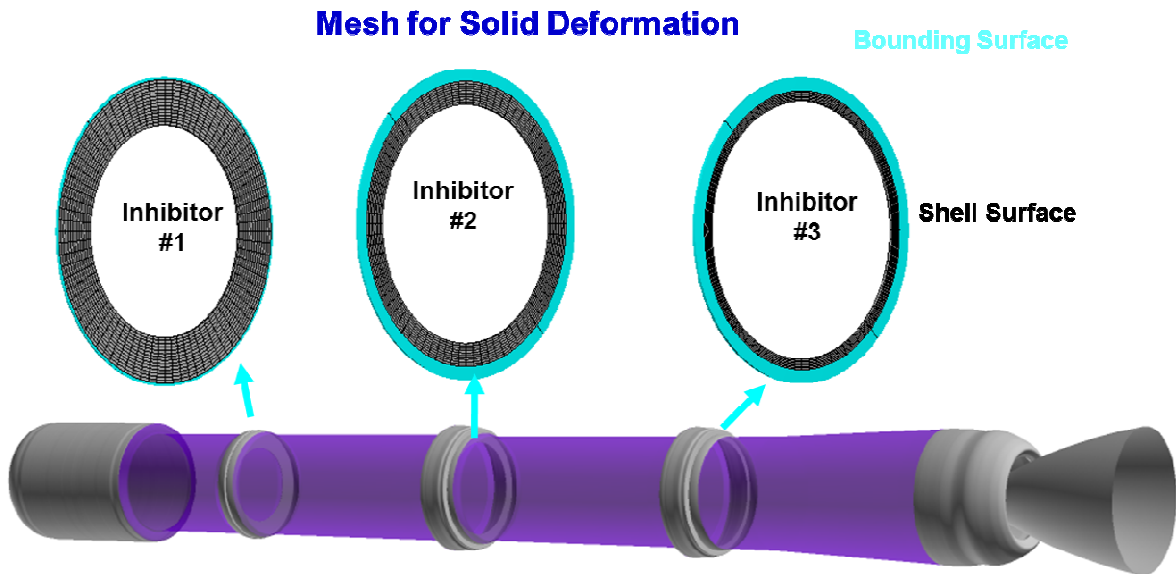

Figure 7. Geometry for RSRM with close-up on flexible inhibitors showing the portion of each inhibitor that is fixed (cyan) and the part that is flexible (black).

D. Structural Dynamics Setting

As can be seen in Figure 7, the bounding surfaces on all three inhibitors are fixed as zero displacement. The 1st inhibitor thus has the largest surface area that is capable of deforming, and the 3rd inhibitor has the smallest. A linear elasticity model is used for the solid material in which the elastic modulus E=1.8x10^{8} Pa,[6,7,9] Poisson ratio ν=0.49998 and density ρ=1,000 kg/m^{3} . Nonlinear large geometrical deformations are permitted. During the initial testing, it was found the above Young's modulus gives excessive deformation of the inhibitor, making a converged solution impossible. It was decided to use larger values of E=1.4x10^{9} Pa, and ρ=7,800 kg/m3. As both Young's modulus and density are increased at the same ratio, this will ensure the same modal frequency of the inhibitors. For the structural solver, a 2nd order accurate temporal scheme of Newmark is used, along with a time step the same as that in the CFD solver of 0.0001s for all simulations.

V. Results

In this section, results for coupled fluid-structure interaction in the RSRM are presented. Results for decouples solutions are presented and discussed first, followed by results for coupled fluid-structure interaction simulations.

A. Fluid Solution with Rigid Inhibitor

In preparation for the fully coupled fluid-structure interaction simulation, we first perform fluid-only simulations with rigid structures to allow the flow inside the solid rocket motor to develop to a nearly fully-developed state. The problem can be very stiff in the beginning, so we employ 1st order schemes to establish the initial flow field. A representative instantaneous flow field from an initial run is shown in Figure 8. The instantaneous Mach number, vorticity and pressure fields are displayed at the top, middle, and bottom of the figure, respectively. As one can see from the Mach number contours, the flow is almost fully developed. The initial flow inside the RSRM is clearly vortex-dominated with heavy vortex shedding present at all of the rigid inhibitors, which locally produce lower pressures due to the vortices as observed just downstream of the first inhibitor. There is also a clear net pressure gradient axially toward the nozzle exit, which will ultimately act to bend the inhibitors in that direction during the coupled FSI simulations.
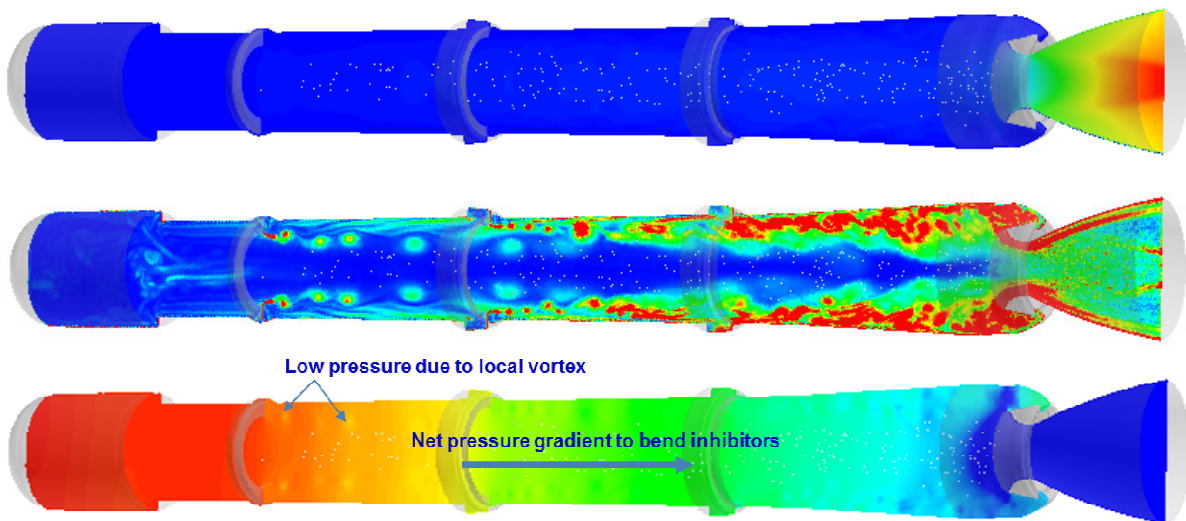

Figure 8. Initial transient CFD solution for RSRM with rigid inhibitors: (Top) Instantaneous Mach number field; (Middle) Instantaneous vorticity field; (Bottom) Instantaneous pressure field.

B. Structural Solution without Fluid Forcing

The current CFD solver Loci/CHEM has been used at NASA MSFC for many years and it has been validated and verified for many different applications. On the other hand, the current structural solver, CoBi, is not particularly well known. To instill some confidence in the structural solver, we will first present two verification cases relevant to the inhibitor: the bending of a circular plate and the first four natural frequencies of the circular plate, as shown in Figure 9. In these two cases, analytical solutions are known and available.
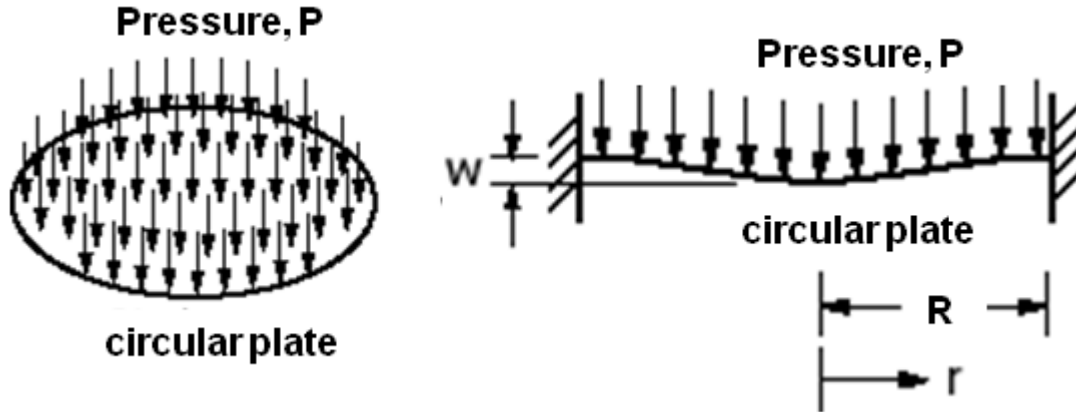
Figure 9. Bending of a circular plate under uniform pressure.

The governing equation for the linear bending of the circular plate under a uniform pressure force P is:[16]

$$\nabla^4 w = \left(\frac{d^2}{dr^2} + \frac{1}{r}\frac{d}{dr} \right)\left(\frac{d^2}{dr^2} + \frac{1}{r}\frac{d}{dr} \right)w = \frac{P}{D} \tag{29}$$

where w is the deflection of the plate, and D is the bending rigidity of the plate,

$$D = \frac{Et^3}{12(1-v^2)} \tag{30}$$

The parameters t and v are the thickness and Poisson's ratio of the plate material, respectively. With a clamped edge boundary:

$$w = 0;\quad \frac{dw}{dr} = 0, \quad \text{at } r=R \tag{31}$$

one can find the analytical solution in the form of:

$$w(r) = \frac{PR^4}{64D}\left[1 - \left(\frac{r}{a}\right)^2 \right]^2 \tag{32}$$

The verification model has the similar geometrical and mesh sizes as the first inhibitor as shown in Figure 10. The computed plate deflection from the CoBi shell element solution is compared with the above analytical solution in Figure 11. As one can see, both solutions are essentially identical.
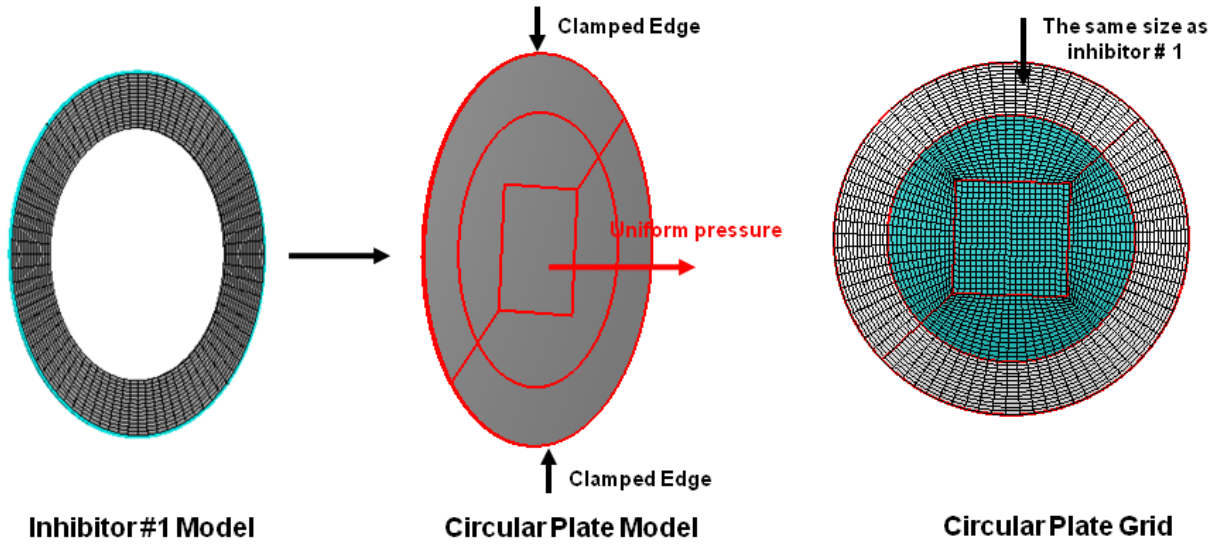
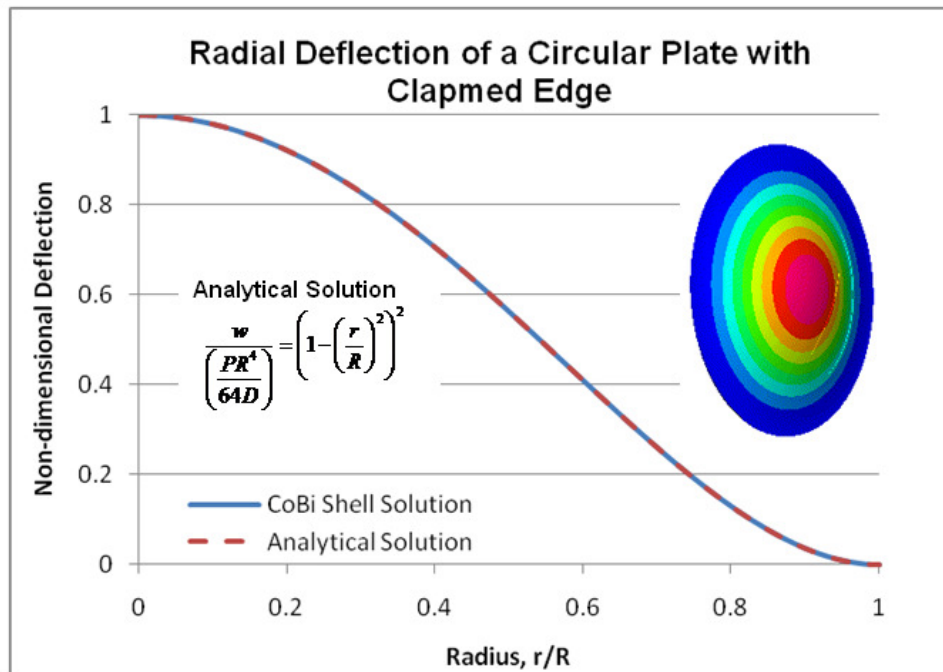**Figure 10. Verification model for circular plate under uniform pressure.**

Figure 11. Comparison between analytical solution and present FEM solution from CoBi.

To find the natural frequency of the above circular plate, the governing equation can be written as:

$$\nabla^4 w + \frac{m}{D} \frac{\partial^2 w}{\partial t^2} = 0 \tag{33}$$

where m is the plate mass per unit area. The eigenvalue solution of the above equation is in the form of Bessel functions:

$$J_0(\gamma R)I_1(\gamma R) + J_1(\gamma R)I_0(\gamma R) = 0 \qquad (34)$$

The first few natural frequencies are:[17]

$$\omega_1 = \frac{k_n}{R^2}\sqrt{\frac{D}{m}} \; ; \; k_1=10.22; \; k_2=21.26; \; k_3=34.88; \; k_4=39.77 \qquad (35)$$

Figure 12 shows the first few modal shapes and frequencies of the circular plate. The analytical solutions for the first 4 modes are compared with the present prediction. Excellent agreements are obtained for several different modes. The results from NASTRAN are also shown in the figure. One can see that CoBi provides superior accuracy.

| 1st mode | 2nd mode | 3rd mode | 4th mode |

Modes	Frequency			Error	
	Analytical (Hz)	NASTRAN (Shell)	CoBi (Shell)	NASTRAN (Shell)	CoBi (Shell)
1st mode (fundamental)	1.867	1.888	1.866	-0.13%	0.033%
2nd mode (one nodal diameter)	3.883	3.928	3.866	-0.17%	-0.077%
3rd mode (two nodal diameters)	6.371	6.435	6.374	-0.46%	-0.053%
4th mode (one nodal circle)	7.264	7.347	7.272	-0.26%	-0.128%
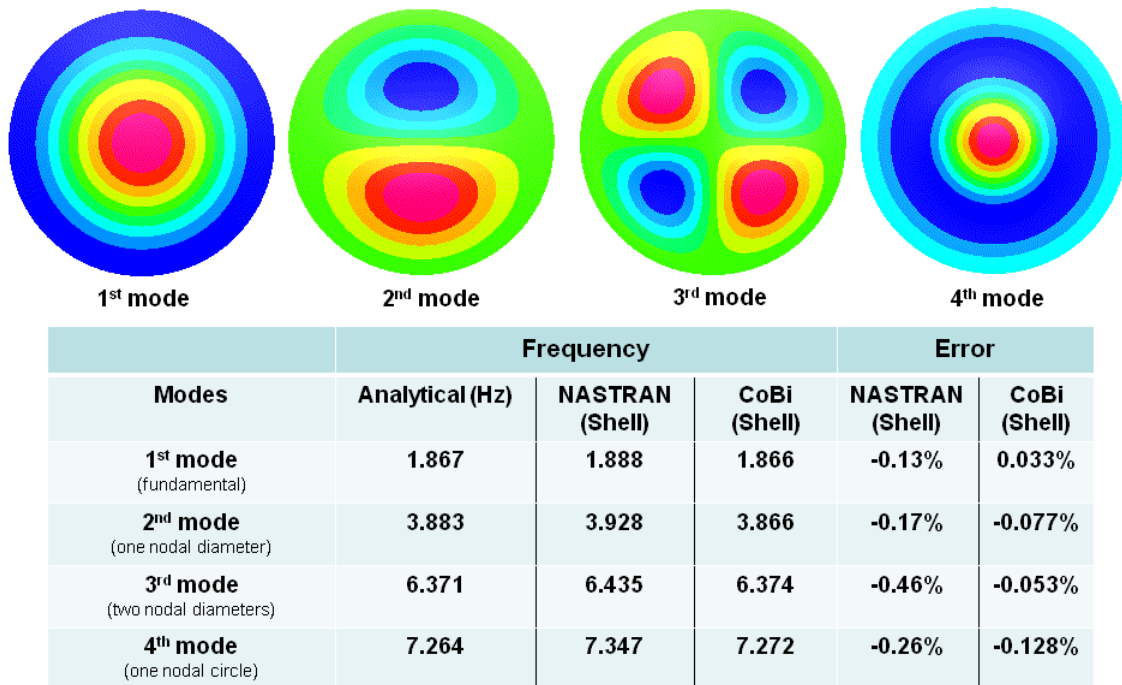
Figure 12. Bending modes of circular plate and comparison with analytical solution and prediction by NASTRAN.

It should be noted that this verification exercise was conducted with the stand-alone CoBi binary constructed from the same source code as is coupled with the Loci/CHEM CFD program for the FSI simulation.

With the above successful verification study, a modal analysis was performed on the first 40 structural modes of the three inhibitors. The computed modal shapes for all three inhibitors are shown in Figure 13. As one can see, the first inhibitor has area large area exposed to the fluid and hence has the lowest natural frequency of 7.62Hz. This mode is axi-symmetric. The mode numbers 2 and 3 are a pair and have the same frequency with a modal shape rotated by 90 deg to the axial direction. The 2nd bending mode of the first inhibitor is mode number 37 and has a frequency of 45.2Hz. The first bending frequency for the second inhibitor is 30.55Hz, and the first bending mode for the third inhibitor is beyond the first 40 modes of the present analysis.
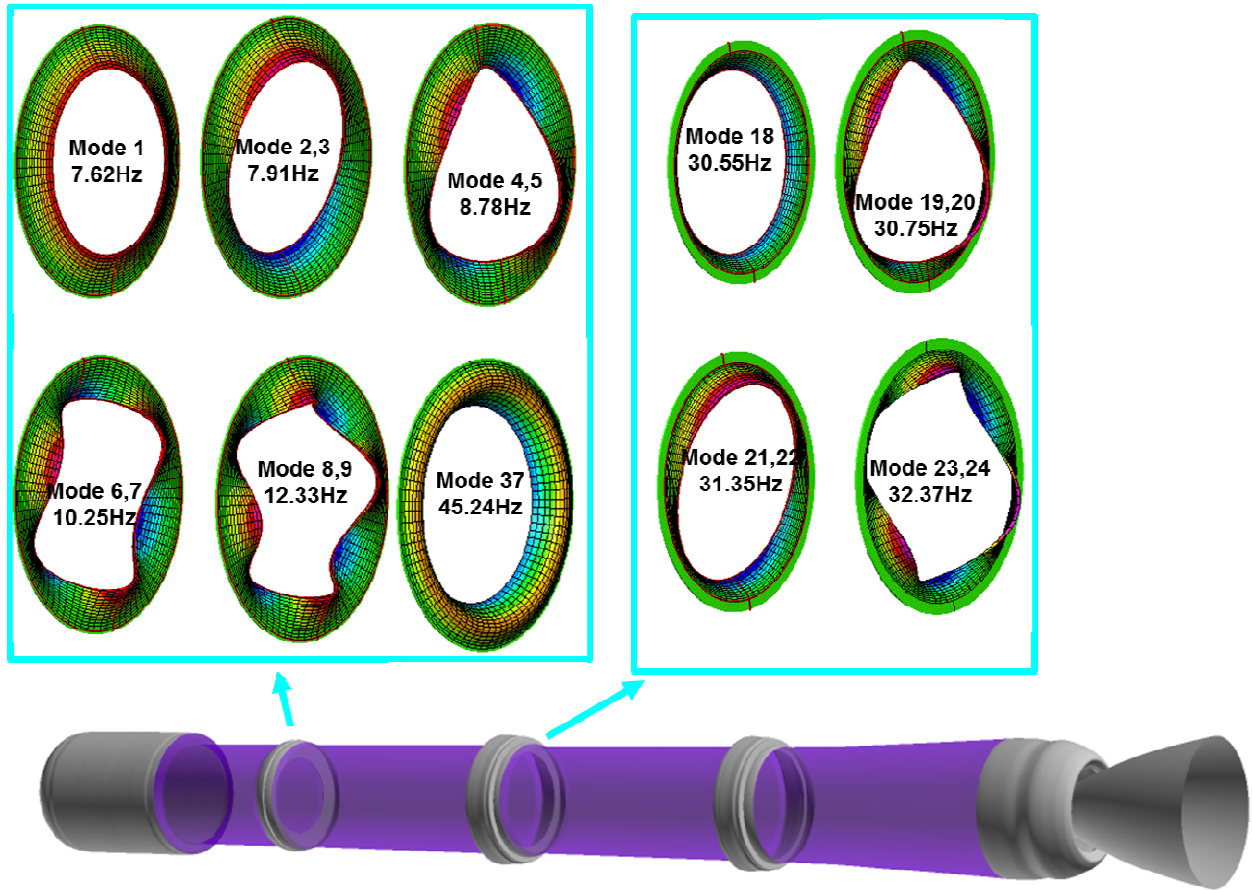
Figure 13. Structural modes for first two RSRM inhibitors computed using CoBi modal analysis.

C. Coupling and Iteration Process

A schematic is shown in Figure 14 to illustrate the iterative workflow of the tightly-coupled fluid-structure interaction process. The flow field is restarted from the previous 1st order solution (but changed to 2nd order in both time and space), and the structural solution is started with no deformation and zero velocity initial conditions. First the structural solver receives the traction force acting on the structural boundary and then solves for the deformation. This deformation is then mapped to fluid surface mesh. The moving mesh deformation is activated to deform the volumetric fluid mesh based on the surface deformation. With this new deformation, the fluid field is solved to obtain a new traction force. This force is then fed to the structural solver again and so on. The fluid and structure are solved in this tightly-coupled manner at every sub-iteration within each time step until convergence is reached in each solver. Typically, the residual from the structural solver drops 3 orders of magnitude within 6 sub-iterations as shown in Figure 15.
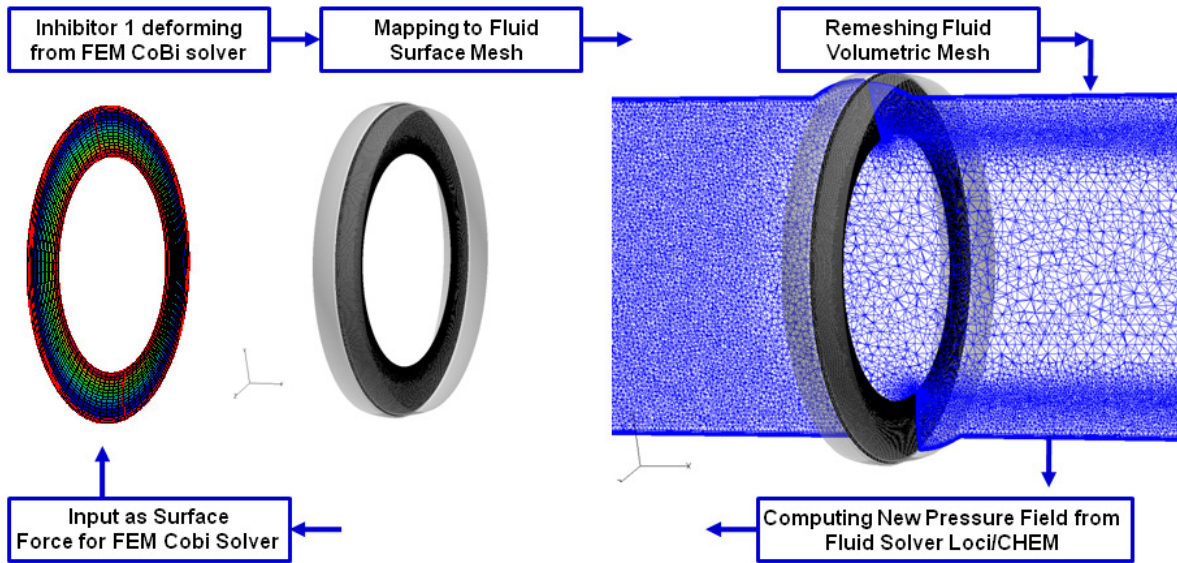
Figure 14. Schematic showing iterative workflow of tightly-coupled fluid-structure interaction process.
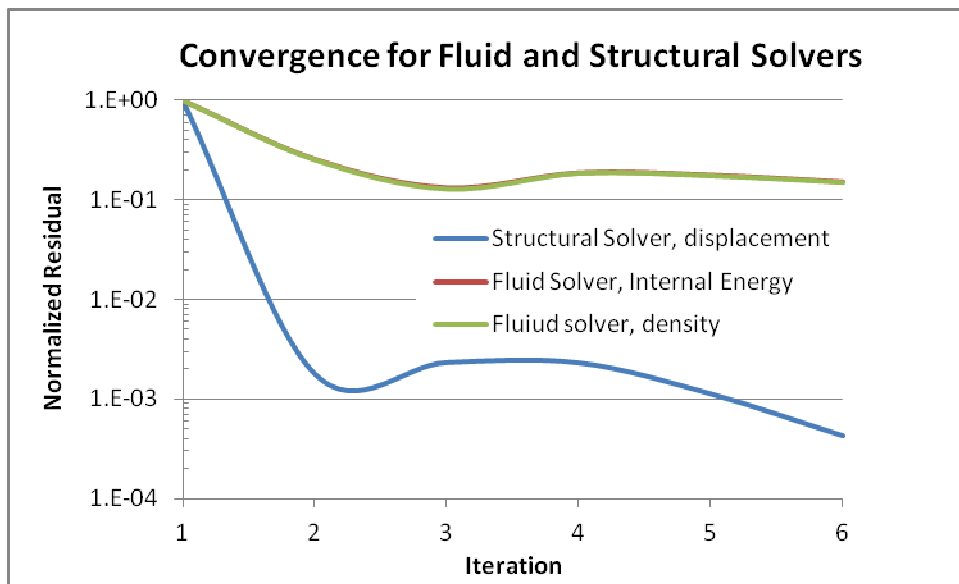

Figure 15. Normalized residual drops for fluid and structural solvers during a typical time step.

D. Coupled Fluid-Structure Solution

Tightly-coupled fluid-structural interaction simulations were carried out for the RSRM application with flexible inhibitors until *t*=0.60s. The instantaneously computed vorticity field on a slice through the RSRM, including the deforming solid surfaces, at six different time instances from 0.1s to 0.6s in even 0.1s increments is shown in Figure 16. Unsteady vortex shedding is clearly observed at each of the flexible inhibitors, and the first inhibitor is undergoing very large deformations in response to the large pressure gradients present within the solid rocket motor.
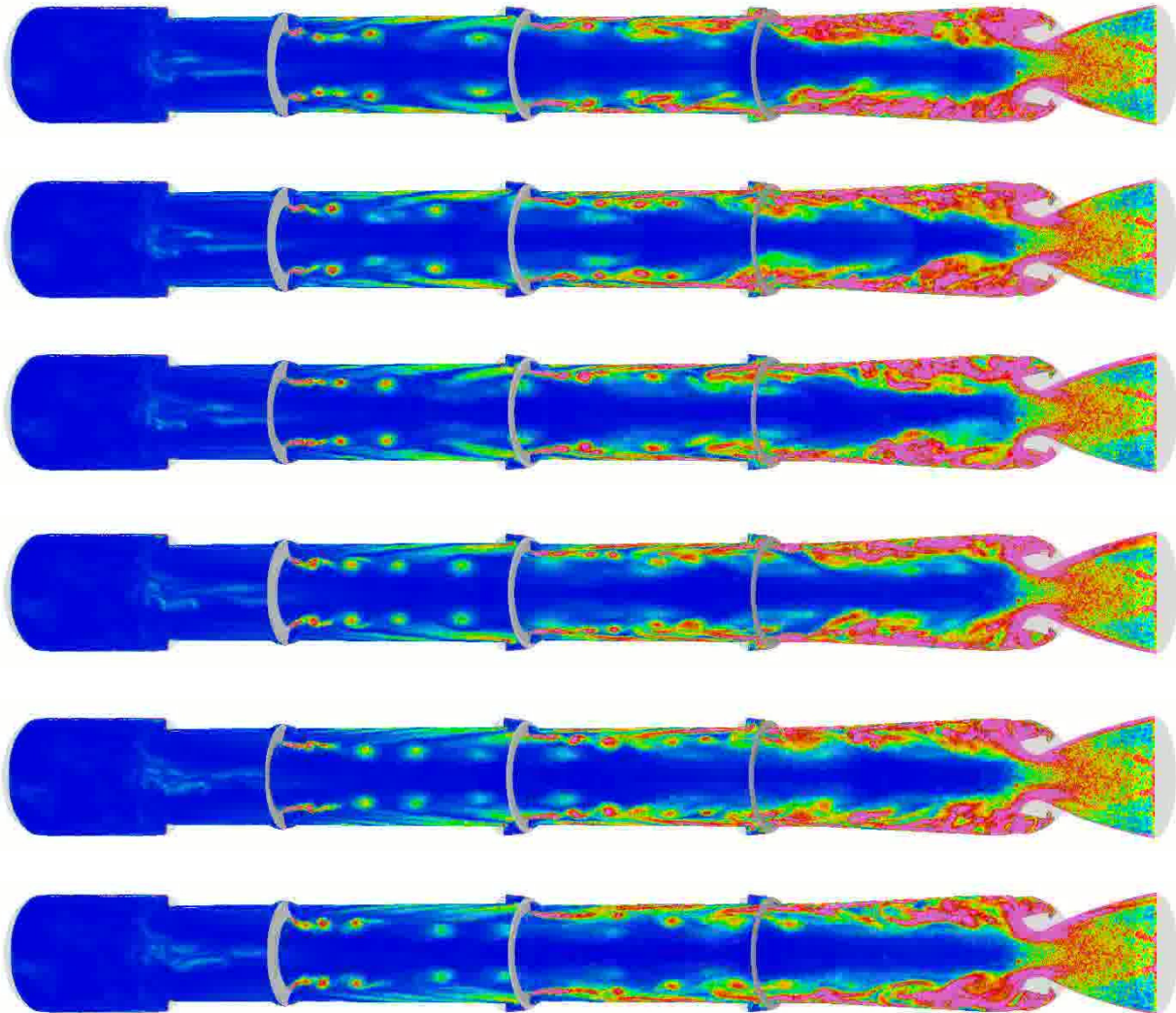
American Institute of Aeronautics and Astronautics

Figure 16. Instantaneous vorticity field for tightly-coupled FSI simulation of RSRM with flexible inhibitors: From 0.1s (Top) to 0.6s (Bottom) in even 0.1s increments.

The large structural deformations are very clearly observed in the close-up views of the first inhibitor along with the fluid mesh colored by vorticity presented in Figure 17. The inhibitor tip can be seen deflecting up to about 20-30 degrees in each direction in response to the unsteady flow with large pressure gradients.
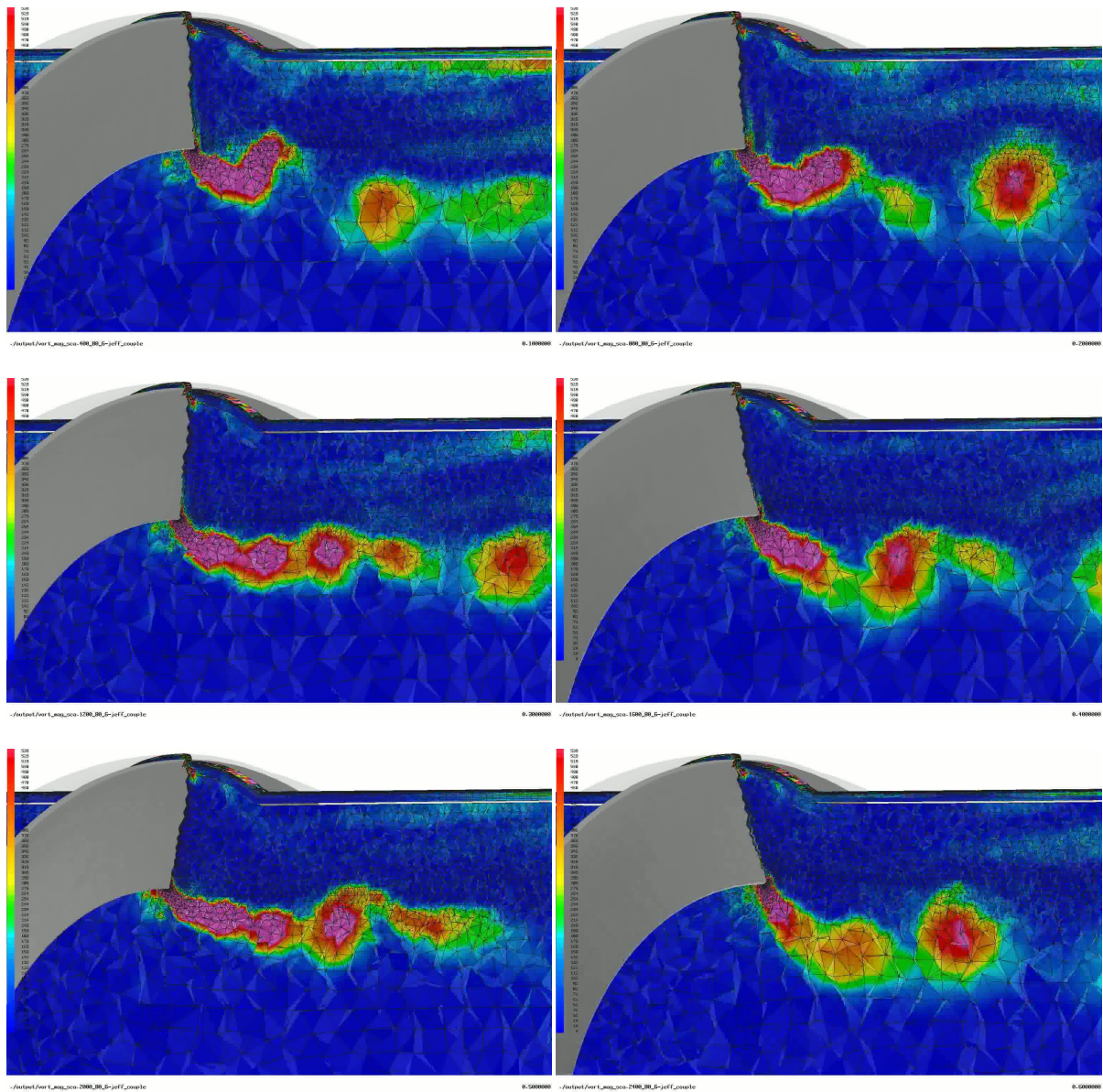
Figure 17. Close-up view of first inhibitor, fluid mesh and instantaneous vorticity field for tightly-coupled FSI simulation of RSRM with flexible inhibitors: From 0.1s (Top left) to 0.6s (Bottom right) in even 0.1s increments.

To show the three-dimensional nature of the unsteady vortical flow, instantaneous iso-surfaces of helicity at three different time instances (0.05s, 0.10s, and 0.15s) are presented in Figure 18. Here the helicity is defined as the dot product of velocity vector with vorticity vector. In response to the periodic unsteady vortex shedding, vortex-vortex interactions, and vortex interactions with flexible inhibitors, the flow becomes increasingly helical as it travels downstream toward the nozzle exit.
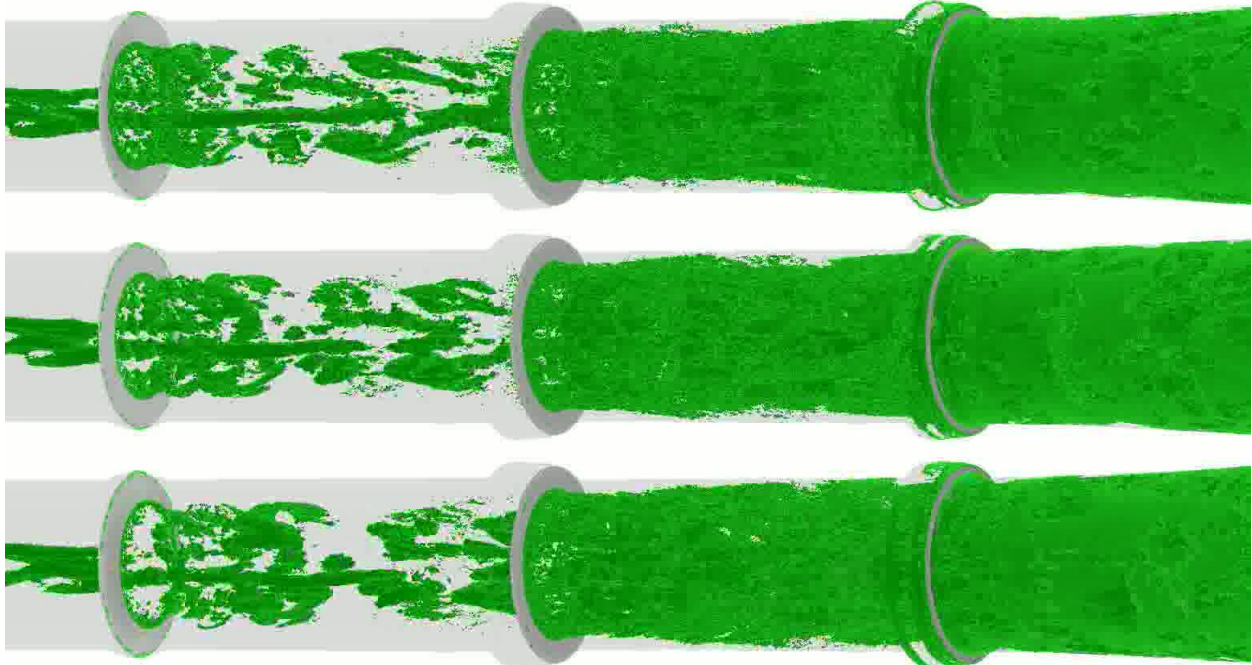
Figure 18. Instantaneous helicity field for tightly-coupled FSI simulation of RSRM with flexible inhibitors: (Top) 0.05s; (Middle) 0.10s; and (Bottom) 0.15s.

Figure 19 displays the time history of the three inhibitor tip displacements from the coupled solution. Due to its small extrusion into the flow field, the 2nd and 3rd inhibitors exhibit very small displacements in response to the flow. The 3rd inhibitor behaves essentially as a rigid body, and the 2nd inhibitor exhibits periodic motion at its own first natural frequency of 30.55Hz (Figure 11).
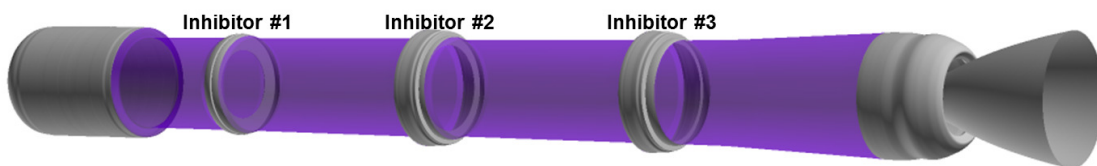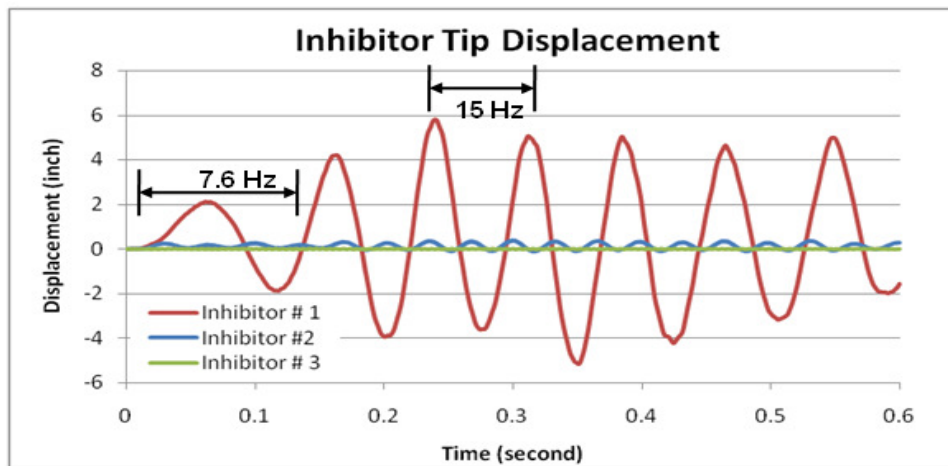

Figure 19. Time history of inhibitor tip displacement showing 1st inhibitor shift from its own first modal frequency (7.5 Hz) to the SRM acoustic frequency (15 Hz).

American Institute of Aeronautics and Astronautics

Due to its flexibility, the 1st inhibitor shows some very interesting dynamics. Initially, the 1st inhibitor oscillates at its own natural frequency of 7.5 Hz, but gradually shifts to the solid rocket motor acoustic frequency of 15Hz. Its motion is driven by the internal acoustic wave in the first mode, and the displacements appear to settle to a periodic motion. As shown in Figure 20, at 15Hz the 1st inhibitor vibrates at its own first modal shape, rather than its own modal shape at 15.2 Hz. This implies that the driving force (or the pressure field) is axi-symmetric. When the inhibitor vibrates at the rocket motor first acoustic modal frequency, it will shed a coherent vortex at 15Hz. It will be interesting to determine its feedback on the acoustic wave amplitude. This will be investigated in the future studies.
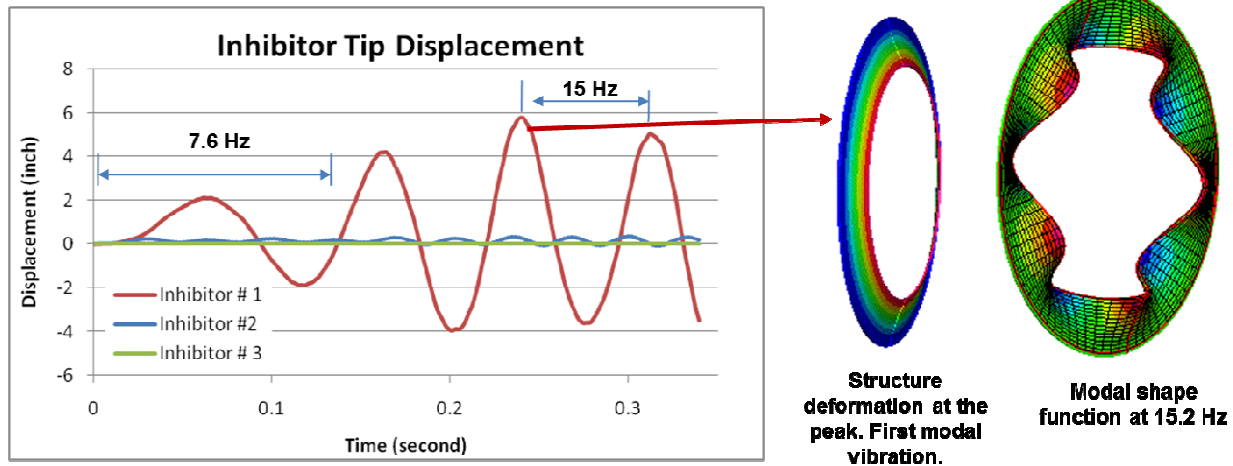

Figure 20. Comparison of structural deformation at the peak tip displacement for the first inhibitor with its computed modal shape at 15.2 Hz.

VI. Summary and Potential Applications

Solving fluid-structure interaction problems requires coupling two totally different solvers: one for computational fluid dynamics (CFD) and one for computational structural dynamics (CSD). The new simulation tool presented here couples the Loci/CHEM CFD solver with the CoBi CSD solver through the interchange of boundary variables across the solid-fluid interface. The tool employs a special time iteration technique to ensure strong coupling between the two solvers. This modular treatment enables the application of well-established and optimized methods for the flow and the structure, respectively. The SLS SRM simulations use a production-level hybrid RANS/LES CFD model with a grid resolution of 80 million cells, and the three flexible inhibitors are modeled with around 2,500 3D shell elements. A new capability to fully couple a production CFD solver (Loci/CHEM) to a structural solver has been demonstrated. Initial results for the flexible inhibitor in the RSRM show a strong coupling of inhibitor dynamics with acoustic pressure oscillations inside the RSRM. This new capability can provide insight to understand the thrust oscillation issues relevant to SLS design. The multi-disciplinary tool can also be readily used to study other fluid-structure interaction phenomena in the SLS propulsion system, such as:

- Liquid propellant tank breathing due to propellant interaction with the flexible tank shell
- Interactions between the water suppression system on the launch pad and ignition overpressure waves during liftoff
- Fluid-induced vibration in delivery pipes with bellows
- Fluid-thermal-structural coupling in rocket engine nozzles
- Cavitation-induced vibration in turbopump inducer blades

VII. Acknowledgements

VIII. References

[1]   McWhorter, B. B., "Real-Time Inhibitor Recession Measurements in Two Space Shuttle Reusable Solid Rocket Motors", AIAA/ASME/SAE/ASEE Joint Propulsion Conference and Exhibit, AIAA-2003-5107, July 2-23, 2003.

[2]   Plourde, F., Najjar, F. M., Vetel, J., Wasistho, B., Doan, K. S., and Balachandar, S., Numerical Simulations of Wall and Shear-Layer Instabilities in a Cold Flow Set-up, 37th AIAA/ASME/SAE/ASEE Joint Propulsion Conference and Exhibit, AIAA-2003-4674, July 20-23 (2003).

[3]   Anthoine, J., and Buchkin, J-M, Effect of Nozzle Cavity on Resonance in Large SRM: Numerical Simulations, J. Propulsion and Power, 19 (3), (2003), pp. 374-384.

[4]   Mason, D. R., Morstaadt, R. A., Cannon, S. M., Gross, E. G., and Nielson, D. B., Pressure Oscillations and Structural Vibrations in Space Shuttle RSRM and ETM-3 Motors, 38th AIAA/ASME/SAE/ASEE Joint Propulsion Conference and Exhibit, AIAA-2004-3898, July 11-14, (2004).

[5]   Mastrangelo, et al., "Segmented SRM Pressure Oscillation Demonstrator", AIAA/ASME/SAE/ASEE 47th Joint Propulsion Conference, 2011. AIAA-2011-6056, 2011.

[6]   Roach, R. L., Gramoll, K. C., Weaver, M. A, and Flandro, G. A., "Fluid-Structure Interaction of Solid Rocket Motor Inhibitors", 28th AIAA/ASME/SAE/ASEE Joint Propulsion Conference and Exhibit, AIAA-92-3677, July 6-8 (1992).

[7]   Weaver, M. A., Gramoll, K. C., and Roach, R. L., "Structural Analysis of a Flexible Structural Member Protruding into an Interior Flow Field", 34th AIAA/ASME/ASCE/AHS/ASC Structures, Structural Dynamics, and Materials Conference, AIAA-93-1446, (1993).

[8]   Fiedler, R., Namazifard, A., Campbell, M., and Xu, F., "Detailed Simulations of Propellant Slumping in the Titan IV SRMUPQM-1,"42nd AIAA/ASME/SAE/ASEE Joint propulsion Conference and Exhibit, Sacramento, CA, AIAA Paper 06-4592, July 2006.

[9]   Wasistho, B., Fiedler, R., Namazifard, A., and Mclay, C., "Numerical Study of Turbulent Flow in SRM with Protruding Inhibitors", 42nd, AIAA/ASME/SAE/ASEE Joint Propulsion Conference & Exhibit, 9-12, July, 2006, Sacramento, CA., AIAA-2006-4589, 2006.

[10] Harris, R. and Luke, E. "Development and Validation of a Fluid-Structure Interaction Capability in the Loci/CHEM solver", 51st AIAA Aerospace Science Meeting, 7-10 January 2013, Grapevine, TX, AIAA-2013-0099.

[11] Luke, E. and George, T., "Loci: "A Rule-Based Framework for Parallel Multidisciplinary Simulation Synthesis," Journal of Functional Programming, Special Issue on Functional Approaches to High-Performance Parallel Programming, Vol. 15, No.3, 2005, pp. 477-502.

[12] Luke, E., "On Robust and Accurate Arbitrary Polytope CFD Solvers (Invited),"AIAA 2007-3956, AIAA Computational Fluid Dynamics Conference, Miami, 2007.

[13] Liu, Q., Luke, E., and Cinnella, P., "Coupling Heat Transfer and Fluid Flow Solvers for Multi-Disciplinary Simulations," AIAA Journal of Thermophysics and Heat Transfer, Vol. 19, No. 4, 2005, pp 417-427.

[14] Roy, C., Tendean, E., Veluri, S.P., Rifki, R., Luke, E., and Hebert, S., "Verification of RANS Turbulence Models in Loci-CHEM using the Method of Manufactured Solutions", 18th AIAA Computational Fluid Dynamics Conference, 25-28 June, 2007, Miami, FL. AIAA-2007-4203.

[15] Davis, P., Tucker, P. K., and Kenny, R. J., "RSSM Thrust Oscillations Simulations", Presented at the JANNAF 2011 MSS/LPS/SPS Joint Subcommittee Meeting, Huntsville, AL, 12/08/2011.

[16] Rilkey, W.D., Formulas for Stress, Strain, and Structural Matrices, John Wiley and Sons, Inc., 1994. ISBN 0471527467.

[17] Yang, H. Q and West, J. "Computational Fluid Dynamics Analysis of J-2X LOX Inducer Modal Damping", ER42(12-097)/ESTSG-FY12-623, 2012.

American Institute of Aeronautics and Astronautics